
***RoboUniView*: Visual-Language Model with Unified View Representation for Robotic Manipulation**

Fanfan Liu
Meituan
Beijing, China 100012
liufanfan03@meituan.com

Feng Yan
Meituan
Beijing, China 100012
yanfeng05@meituan.com

Liming Zheng
Meituan
Beijing, China 100012
zhengliming04@meituan.com

Chengjian Feng
Meituan
Shenzhen, China 518110
fengchengjian@meituan.com

Yiyang Huang
Meituan
Beijing, China 100012
huangyiyang02@meituan.com

Lin Ma*
Meituan
Beijing, China 100012
malin11@meituan.com

Abstract

Utilizing Vision-Language Models (VLMs) for robotic manipulation represents a novel paradigm, aiming to enhance the model’s ability to generalize to new objects and instructions. However, due to variations in camera specifications and mounting positions, existing methods exhibit significant performance disparities across different robotic platforms. To address this challenge, we propose *RoboUniView* in this paper, an innovative approach that decouples visual feature extraction from action learning. We first learn a unified view representation from multi-perspective views by pre-training on readily accessible data, and then derive actions from this unified view representation to control robotic manipulation. This unified view representation more accurately mirrors the physical world and is not constrained by the robotic platform’s camera parameters. Thanks to this methodology, we achieve state-of-the-art performance on the demanding CALVIN benchmark, enhancing the success rate in the $D \rightarrow D$ setting from 93.0% to 96.2%, and in the $ABC \rightarrow D$ setting from 92.2% to 94.2%. Moreover, our model exhibits outstanding adaptability and flexibility: it maintains high performance under unseen camera parameters, can utilize multiple datasets with varying camera parameters, and is capable of joint cross-task learning across datasets. Code is provided for re-implementation. <https://github.com/liufanfanlff/RoboUniview>

1 Introduction

Recent developments in foundation models [41, 12, 48] show significant advancements, demonstrating robust capabilities across a diverse array of tasks such as visual question answering (VQA) [56], open-vocabulary object detection and segmentation [30, 16, 43], and comprehensive text-image understanding [50]. These achievements unequivocally motivate continued research into the effective integration of these models’ capabilities into robotic control systems.

*Lin Ma is the corresponding author.



Figure 1: The visualization of *RoboUniView* on $D \rightarrow D$ split. The first row shows the predicted occupancy, and the second row shows the predicted rollouts.

Building on this momentum, the academic community diverge into two prominent methodologies: The first approach utilizes prompt tuning of out-of-the-box Large Language Models (LLMs) and Vision Language Models (VLMs) for zero-shot planning and task decomposition, which is subsequently complemented by the activation of a low-level skill library [1, 13, 20, 37, 44, 51]. These methods require intricate prompt tuning and strategic logic. The second approach focuses on imitation learning or reinforcement learning, using extensive robotic datasets [6, 5, 28, 26, 3]. Drawing on the development trajectory of autonomous driving technology [19, 52, 34, 22], these methods hold greater potential for achieving general intelligence in the field of robotic manipulation. However, existing methods exhibit significant performance disparities across different robotic platforms about the second approach. One of the main reasons is the differences in camera specifications and installation positions, which make it difficult for the models to accurately understand the real physical space from varied images, thus affecting the accuracy of their action predictions. We validate this with the state-of-the-art method, RoboFlamingo [28], and find that merely changing the camera parameters during inference cause a significant drop in success rate, from 86.3% to 80.8%. Although some methods are attempting to address this issue, such as RT-X [31], which trains models with more data collection, and 3D Diffusion Actor [26], which adds depth or point clouds to the input, but these approaches undoubtedly increase the workload and hardware costs.

To address such limitations, this paper introduces *RoboUniView*, a novel Visual-Language model with a unified view representation for robotic manipulation. Specifically, it decouples visual feature extraction from action learning. For visual feature extraction, it unifies the multi-perspective views into a unified view representation. To achieve this, we are inspired by BEVFormer [29] and propose a plug-and-play plugin called UVFormer, which can be integrated into any multi-modal model. This plugin is pre-trained on 3D occupancy task, taking multi-perspective views and corresponding camera parameters as inputs, and outputs the occupancy status and RGB values of each cell in

the 3D grid, and gains a deeper understanding of the real physical world. It is noteworthy that our pre-training task only requires simple RGB-D images and does not need expensive manually annotated labels (such as semantic segmentation, objects, actions, etc.). For action learning, it directly outputs robotic actions from the unified view representation, following the design of OpenFlamingo [2] and RoboFlamingo [28], which leverage publicly available pre-trained VLMs to integrate visual and language information.

A substantial amount of experimental evidence demonstrates that our model better comprehends the real physical world and significantly outperforms all existing methods in terms of performance. It also exhibits strong generalizability, maintaining high performance even in robots with unseen camera parameters. On the CALVIN [36] dataset, a widely recognized simulation benchmark for long-horizon language-conditioned tasks, *RoboUniView* establishes a new state-of-the-art by increasing the success rate from 88.7% to 96.2% in the $D \rightarrow D$ setting, from 82.4% to 94.2% in the $ABC \rightarrow D$ setting. Moreover, our model exhibits outstanding adaptability and flexibility: it maintains high performance under unseen camera parameters, can utilize multiple datasets with varying camera parameters, and is capable of joint cross-task learning across datasets. The visualizations are shown in the Figure 1, where *RoboUniView* can capture the real physical environment and output effective actions.

To our knowledge, *RoboUniView* represents the pioneering effort to demonstrate that a unified view representation, when coupled with pre-training on 3D occupancy task, significantly enhances both the performance and generalization capabilities of robotic manipulation across various camera parameters. The main contributions of this paper include: (1) Proposing a Visual-Language model with unified view representation for robotic manipulation, enhancing performance and generalization to robotic camera parameters. (2) proposing an effective pre-training method for obtaining a unified view representation to better comprehend the real physical world; (3) conducting extensive experiments to evaluate the performance of *RoboUniView* in various settings, achieving state-of-the-art performance with a significant advantage on the CALVIN [36] benchmark.

2 Related Work

Language-conditioned Visuomotor Policies. language-conditioned visuomotor robotic are the closest to human-like robotic operation, requiring robots to understand human commands and complete a variety of tasks based on visual feedback. This approach has a wide range of application prospects and challenges; therefore, in recent years, language-conditioned visuomotor policies have received considerable attention. Numerous works involve learning strategies and predictive models for robotic grasping [17, 55, 54, 11, 35, 33]. Robotic learning has seen rapid development in the areas of multi-tasking and language-conditioned learning, and *RoboUniView* is built upon the foundation of these works.

View Transform. View transformation has a wide range of applications in embodied AI, with the goal of converting perspective view features into a unified view aligned with the target task. In autonomous driving tasks, perception and planning need to be conducted from a Bird’s Eye View (BEV) perspective. A direct method is to transform the perspective view into BEV using Inverse Perspective Mapping (IPM) [42, 7]. Additionally, Lift-Splat [40] generates BEV features based on depth distributions, while BEVFormer [29] utilizes a Transformer to learn the conversion from perspective view features to BEV features. PETR [32] utilizes 3D positional encoding to implicitly complete view transformation. Subsequent work like UNIAD [19] completes end-to-end autonomous driving control based on View Transformation. In the field of robotic control, RVT [15] converts multiple perspective views into orthogonal perspective views, and VIHE [49] transforms multiple perspective views into a hand-centric view. However, these works’ viewpoint transformations rely on real depth and are still within a perspective view, leading to a mismatch between visual features and action space. In contrast, our work does not rely on depth maps and converts perspective view features into a unified 3D space view, aligning visual features with the action space.

Generalization in robot learning. In the field of robotic learning, developing robotic controllers that can generalize across a variety of scenarios has been a long-standing research objective[24]. Previously, some researchers have improved the generalization capabilities of robotic controllers by training models on a large and diverse datasets. For instance, tasks involving unseen objects [53, 27, 14], new combinations of objects and skills [8, 21], new language instructions [23, 38], and

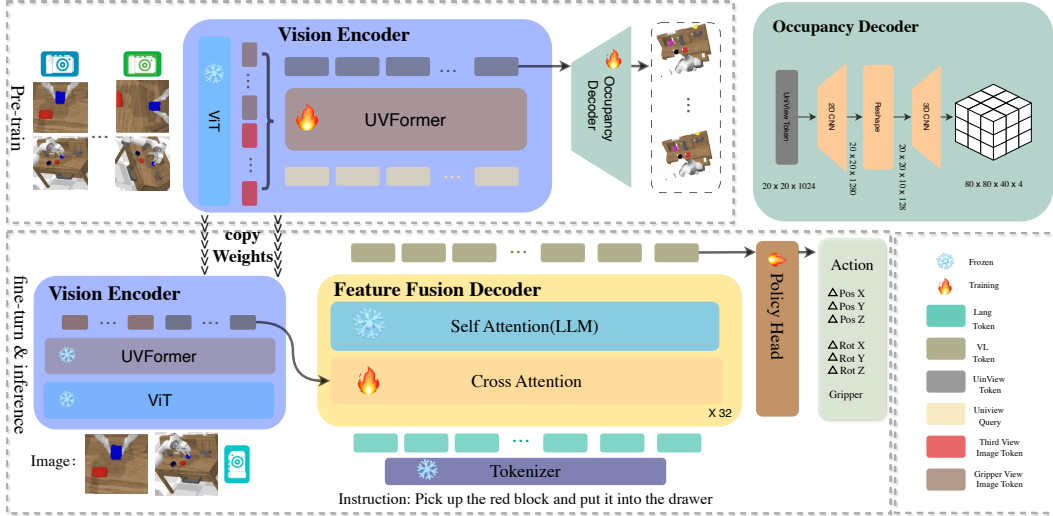


Figure 2: Overview of the *RoboUniView*. *RoboUniView* is first pre-trained on the 3D occupancy task, and then fine-tuned on robot data to learn multi-task visual robot manipulation.

new semantic object categories [45]. Unlike these earlier efforts, recent works like RT2 [5] and RoboFlamingo [28] have utilized pre-trained models to enhance generalization capabilities, with these pre-trained models being trained on datasets much larger than those typically used for robots. Despite these advancements, current methods still focus on the capabilities for a single robotic embodiment. When the camera parameters of the robotic embodiment changes, the model non-functional. The goal of our method is to leverage the capabilities of pre-trained models while also being able to learn skills on data from robots with different camera parameters, ultimately achieving generalization of a single model to different camera-configured robotic embodiment.

Pre-training for robotic manipulation. Pre-training technology has driven the advancement of the entire artificial intelligence industry, ranging from early applications of various backbones pre-trained with supervised learning on ImageNet [9] for basic visual tasks, to large language models using self-supervised pre-training [10], and multi-modal models pre-trained with contrastive learning [41]. In the field of robotic learning, previous researchers have also explored the use of pre-training techniques to enhance visual encoders [25]. Additionally, some work has employed pre-trained language models as instruction encoders or high-level planners [1, 13, 20, 37, 44, 51]. Recently, some researchers have used pre-training tasks related to robotic control to enhance the end-to-end capabilities of models, with RT2 [5] and RoboFlamingo [28] utilizing pre-trained VLMs. Unlike previous work, we not only utilize pre-trained VLM models, but we have also designed a novel pre-training approach to enhance the model’s understanding of the real physical world.

3 Method

The entire *RoboUniView* framework is illustrated in Figure 2. During the forward process, multi-perspective images pass through Vision Encoder to extract wrist image features and the unified view representation. These are then combined with language tokens in the Feature Fusion Decoder to extract integrated vision-language features. Finally, these features pass through the policy head to execute robotic manipulation. The training process consists of two phases: during the pre-training phase, Vision Encoder undergoes training on a large dataset of easily accessible RGB-D images to learn robust unified view representation; during the fine-tuning phase, the model learns to predict robotic actions from the unified view representation, using paired images and action data.

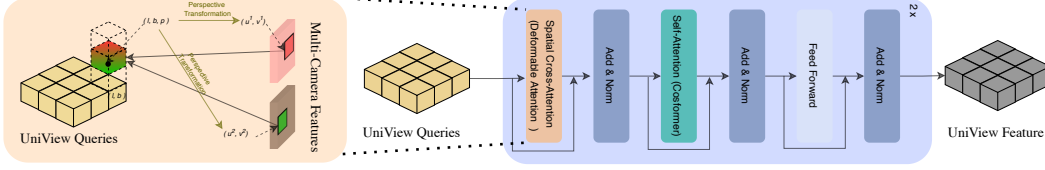


Figure 3: UVFormer which contain grid-shaped UniView queries, Spatial Cross-Attention, and Self-Attention. Within the Spatial Cross-Attention, each UniView query interacts only with the image features of the pixel coordinates projected by its corresponding P 3D points.

3.1 Architecture

3.1.1 Vision Encoder

Our Vision Encoder comprises two parts: the Vision Transformer (ViT) and UVFormer. UVFormer’s primary function is to transform multi-camera perspective view features, as outputted by the Vision Transformer (ViT), into unified view representation features.

Vision Transformer. We utilize pre-trained Vision Transformer (ViT) from CLIP [41] as the image backbone to extract features from images:

$$X_t = \text{ViT}(I_t), \quad (1)$$

where $I_t \in \mathbb{R}^{N \times H \times W \times 3}$ and $X_t \in \mathbb{R}^{N \times H' \times W' \times C}$ represent the N multi-perspective images and their corresponding extracted features at each time step t , respectively. The dimensions $H \times W$ denote the size of the images, and $H' \times W'$ denote the dimensions of the output feature maps.

UVFormer. Inspired by BEVFormer[29], we design a simplified structure called UVFormer, which takes image features X_t , camera parameters Cam , and learnable UniView Queries Q as inputs, and outputs a unified view representation UF_t . The process is defined by the equation:

$$UF_t = \text{UVFormer}(Q, X_t, Cam). \quad (2)$$

$Q = \{Pos, Emb\}$, where $Pos \in \mathbb{R}^{L \times B \times 3P}$ and $Emb \in \mathbb{R}^{L \times B \times C}$ respectively represent the positions and learnable features of the queries, and L, B, P define the spatial shape of the 3D grid located in the robot’s operable space. Here, we set both L and B to be 20. Specifically, $Emb^{l,b} \in \mathbb{R}^C$ is responsible for the corresponding pillar cell region in the unified view space. Each pillar cell corresponds to size of 0.05^2 meters in the real world, with P 3D points uniformly distributed within 0.5-meter range along its vertical direction. Cam represents the camera parameters of N perspectives. $UF_t \in \mathbb{R}^{L \times B \times C}$ is the unified view representation, which encapsulates all relevant information across the $L \times B \times P$ 3D grid.

As shown in Figure 3, UVFormer includes two standard encoders. Each encoder layer consists of a Spatial Cross-Attention, a Self-Attention, and two Feed-Forward Networks (FFN). In the Spatial Cross-Attention layer, we utilize Deformable Attention (DeformAttn) [57] due to the high computational cost associated with the standard multi-head attention mechanism. This resource-efficient attention layer allows each query $Q^{l,b}$ to interact only with the features at specific positions under different camera perspectives, which are determined by the pixel positions resulting from the Perspective Transformation (Proj) of the corresponding P 3D points. The Spatial Cross-Attention (SCA) process is mathematically formulated as follows:

$$\text{SCA}(Q^{l,b}, X_t, Cam) = \frac{1}{N} \sum_{n=1}^N \text{DeformAttn}(Emb^{l,b}, \text{Proj}(Pos^{l,b,P}, Cam^n), X_t^n). \quad (3)$$

In the Self-Attention layer, we implement an attention mechanism that omits the softmax function, providing performance that is comparable to traditional attention methods but with reduced resource consumption.

3.1.2 Feature Fusion Decoder

The Feature Fusion Decoder follows the design of OpenFlamingo[2] and RoboFlamingo[28], taking UF_t, X_t^{wrist} , from the Vision Encoder, and language tokens $L_t \in \mathbb{R}^{I \times C}$ as inputs to generate

vision-language features $VL_t \in \mathbb{R}^{I \times C}$. The entire structure includes L layers of the decoder, each comprising a Cross Attention and Self Attention layer. Where the Self Attention is directly copied from pre-trained language models such as LLaMA[47], GPT-Neox[4], or MPT[46]. The Cross Attention layer uses L_t as queries and the concatenated UF_t and X_t^{wrist} as keys and values, and is fine-tuned on action data through imitation learning. Notably, UF_t and X_t^{wrist} are reshaped into $LB \times C$ and $H'W' \times C$ respectively. When features from the wrist perspective are missing in the data, they can be obtained through reconstruction to generate virtual X_t^{wrist} from other perspectives.

3.1.3 Policy Head

The Policy Head further transforms the output VL_t into the pose of a 7-degree-of-freedom end-effector and the state of the gripper, which includes a Max-Pooling operation to aggregate information along the I dimension, an LSTM[18] to integrate historical vision-language features, and MLP:

$$a_t^{pose}, a_t^{gripper} = \text{MLP}(\text{LSTM}(\text{MaxPooling}(X_{VL}^t), h_{t-1})) \quad (4)$$

where h_{t-1} represents the hidden state at time t , and a_t^{pose} and $a_t^{gripper}$ are the predicted pose of the end-effector and the state of the gripper, respectively.

3.2 Training

3.2.1 Pre-training

In the pre-training phase, we can use any data that includes RGB-D and corresponding camera parameters, rather than relying on expensive and high-quality datasets like RT-X[39]. In this study, we initially adjust the robot platform’s camera parameters within the CALVIN [36] simulation environment to collect diverse RGB-D images. Subsequently, these images, along with their corresponding camera parameters, are used to generate RGB-enriched point clouds, which are then voxelized. This dataset is designated as *Calvin_{rgb-d}*.

As shown in Figure 2, to ensure that the unified view representation extracted by the Vision Encoder contains accurate physical information, we design a very simple occupancy decoder structure using pure convolution. This pre-training process takes multi-perspective RGB images and corresponding camera parameters as inputs, and outputs the occupancy and the RGB values of each grid cell. Here, we employ the L1 loss to supervise the RGB output of each grid cell and the cross-entropy loss to monitor the occupancy of the grid:

$$l_{pre-train} = \lambda_{rgb} l_1^{rgb} + l_{ce}^{occ}, \quad (5)$$

where λ_{rgb} corresponds to the weight, balancing RGB loss l_1^{rgb} and occupancy loss l_{ce}^{occ} .

3.2.2 Fine-tuning

After pre-training, we obtain a robust unified view representation containing physical space information. To effectively control the robot, we simply fine-tune the Feature Fusion Decoder and Policy Head modules on multi-task grasping data to enable them to output specific actions. These actions include the position ($a_t^{pose} = \{\Delta pos_t^x, \Delta pos_t^y, \Delta pos_t^z, \Delta rot_t^x, \Delta rot_t^y, \Delta rot_t^z\}$) of the 6-degree-of-freedom end-effector, as well as the gripper status $a_t^{gripper}$.

During this process, we use maximum likelihood imitation learning. Specifically, we use Mean Squared Error (MSE) loss to optimize the relative position and Binary Cross-Entropy (BCE) loss to optimize the gripper status :

$$l_a = \sum_t (\text{MSE}(a_t^{pose}, \hat{a}_t^{pose}) + \lambda_{gripper} \text{BCE}(a_t^{gripper}, \hat{a}_t^{gripper})), \quad (6)$$

where $\lambda_{gripper}$ corresponds to the weight of gripper status loss, $\hat{a}_t^{pose}, \hat{a}_t^{gripper}$ is the demonstration for end-effector pose and gripper status at timestep t .

Table 1: *RoboUniView* Benchmark Results. We compare average success rates between our model and prior benchmarks on multitask long-horizon control for 34 disparate tasks. A total of 1000 episodes are evaluated, each containing five consecutive tasks.

Method	Train \rightarrow Test	Task Completed in a Sequence					Avg Len
		1	2	3	4	5	
MCIL	$D \rightarrow D$	0.764	0.488	0.301	0.181	0.093	1.820
GCBC	$D \rightarrow D$	0.647	0.284	0.122	0.049	0.013	1.110
LCD	$D \rightarrow D$	0.887	0.699	0.545	0.427	0.322	2.880
SPIL	$D \rightarrow D$	0.846	0.651	0.508	0.380	0.286	2.640
HULC	$D \rightarrow D$	0.827	0.649	0.504	0.385	0.283	2.640
RoboFlamingo	$D \rightarrow D$	0.860	0.714	0.585	0.460	0.349	2.968
HULC++	$D \rightarrow D$	0.930	0.790	0.640	0.520	0.400	3.3
<i>RoboUniView</i> (Ours)	$D \rightarrow D$	0.962	0.888	0.776	0.666	0.563	3.855
MCIL	$ABC \rightarrow D$	0.304	0.013	0.002	0.000	0.000	0.400
SPIL	$ABC \rightarrow D$	0.742	0.463	0.276	0.147	0.080	1.710
HULC	$ABC \rightarrow D$	0.481	0.165	0.057	0.019	0.011	0.670
RT-1	$ABC \rightarrow D$	0.533	0.222	0.094	0.038	0.013	0.900
RoboFlamingo	$ABC \rightarrow D$	0.824	0.619	0.466	0.331	0.235	2.470
GR-1	$ABC \rightarrow D$	0.854	0.712	0.596	0.497	0.401	3.060
3D Diffuser Actor	$ABC \rightarrow D$	0.922	0.787	0.639	0.512	0.412	3.270
<i>RoboUniView</i> (Ours)	$ABC \rightarrow D$	0.942	0.842	0.734	0.622	0.507	3.647

4 Experiments

4.1 Dataset

All our experiments are carried out using the language-conditioned CALVIN dataset [36], which encompasses 34 tasks within four distinct environments (A, B, C, and D). This dataset is developed on the PyBullet simulator and features manipulation scenarios involving a Franka Panda robotic arm. The environments differ in terms of table textures and object placements. CALVIN [36] includes 24 hours of unstructured play data, of which 1% is accompanied by language descriptions. Furthermore, CALVIN [36] assesses 1,000 instruction sequences for sequential tasks, where each task requires the robot to sequentially execute five language instructions. The approach for each subsequent task is guided by a specific target instruction, allowing the agent to advance to the next objective only upon successful completion of the preceding task.

4.2 Comparisons with Other State-of-the-Art Methods

Imitation Performance. We fine-tune *RoboUniView* using the demonstrations from the Split D training set, and evaluate its imitation performance on episodes sampled from Split D ($D \rightarrow D$). It takes about 2 days for training on 8 NVIDIA 80G A100 GPUs. As shown in Table 1, *RoboUniView* significantly outperforms all methods across all metrics. The success rate of task1 is improved from 0.930 to 0.962. Even more impressive, in sequence of consecutive tasks, *RoboUniView* increase the success rate of task5 from 0.400 to 0.563 and raise the average successful sequence length from 3.300 to 3.855. This result is particularly commendable as the complexity and challenge of subsequent tasks significantly increase with the progression of the tasks. This primarily stems from the fact that the initial state of each subsequent task is heavily dependent on the completion state of the previous task, leading to increasingly diverse starting conditions.

Zero-Shot Generalization. We also fine-tune *RoboUniView* on the ABC split and test on the D split ($ABC \rightarrow D$), where the D split presents a completely different visual environment from ABC. It takes about 5 days for training on 8 NVIDIA 80G A100 GPUs. As shown in Table 1, *RoboUniView* improves the success rate of task1 from 0.922 to 0.942, and the average successful sequence length from 3.270 to 3.647, compare to best method. It demonstrate *RoboUniView*'s strong capability in zero-shot generalization.

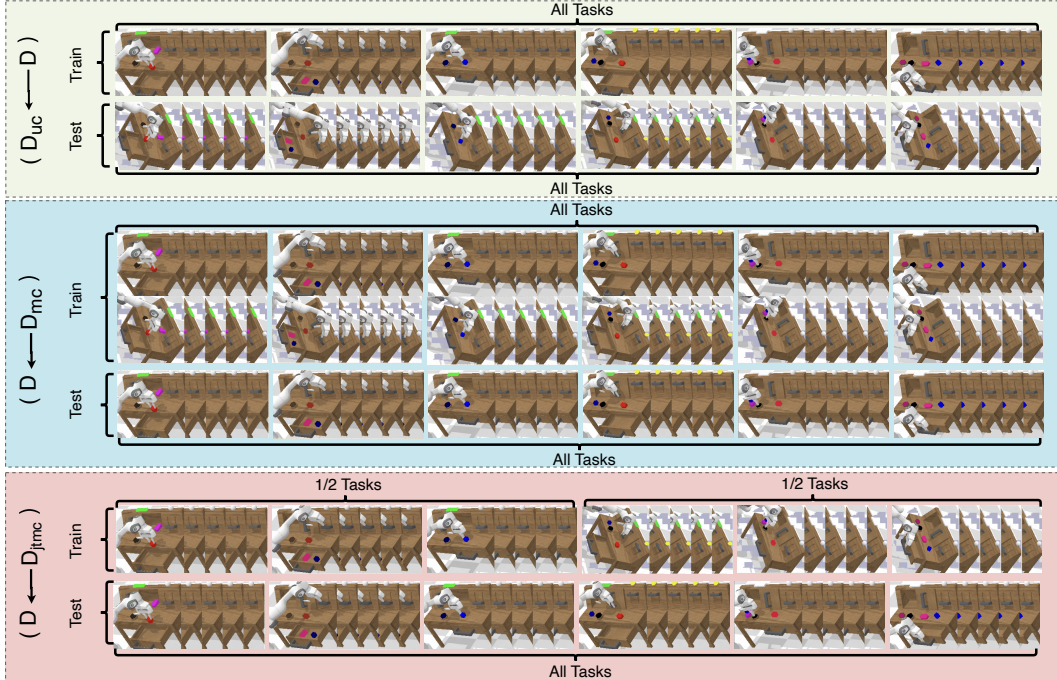


Figure 4: Visualization of environmental configurations in Advanced Experiments.

4.3 Advanced Experiments

To further validate the effectiveness of our method, we conduct three meaningful experiments using RoboFlemingo [28] as the baseline. (1) $D \rightarrow D_{uc}$: Training on the D split and testing on the D split with altered camera parameters. (2) $D_{mc} \rightarrow D$: Training on the D split with two different sets of camera parameters, and testing on the D split. (3) $D_{jtmc} \rightarrow D$: Training on the D split with two different sets of camera parameters, each set of which contain different tasks, and testing all tasks on the D split. It takes about 3 days for training on 8 NVIDIA 80G A100 GPUs. For more detailed information, please refer to Figure 4.

Table 2: Advanced experiments results.

	Method	Train \rightarrow Test	Task Completed in a Sequence					Avg Len
			1	2	3	4	5	
A1	Baseline	$D \rightarrow D$	0.860	0.714	0.585	0.460	0.349	2.968
A2	<i>RoboUniView</i>	$D \rightarrow D$	0.954	0.827	0.685	0.564	0.461	3.491
B1	Baseline	$D \rightarrow D_{uc}$	0.808	0.602	0.427	0.283	0.203	2.323
B2	<i>RoboUniView</i>	$D \rightarrow D_{uc}$	0.956	0.825	0.681	0.561	0.460	3.483
C1	Baseline	$D_{mc} \rightarrow D$	0.821	0.706	0.568	0.441	0.325	2.861
C2	<i>RoboUniView</i>	$D_{mc} \rightarrow D$	0.962	0.888	0.776	0.666	0.563	3.855
D1	Baseline	$D_{jtmc} \rightarrow D$	0.812	0.622	0.472	0.349	0.254	2.509
D2	<i>RoboUniView</i>	$D_{jtmc} \rightarrow D$	0.966	0.859	0.703	0.590	0.473	3.591

Zero-Shot Unseen Camera Parameters Generalization. To validate the generalization ability of *RoboUniView* for zero-shot unseen camera parameters, we train both our model and the baseline on the D split, and subsequently test them on D split ($D \rightarrow D_{uc}$) with different camera parameters compare to training set. As illustrated in rows B1 and B2 of Table 2, our method achieves high success rate of 0.956 in task1, significantly surpassing the baseline’s 0.808. In comparison to rows A1 and A2, our method exhibits minimal fluctuation in success rate, less than 0.004 (0.681 vs 0.685) for all tasks, while the baseline method shows substantial variability, ranging from 0.052 (0.808 vs

0.860) to 0.177 (0.283 vs 0.460). This robust generalization capability is attributed to our unified view representation, which consistently maintains stable output.

Training on Multi Different Camera Parameters Datasets. We re-render images based on D split training set with altered camera parameters, and merge them with the original D split training set to form the D_{mc} training set. We train our model and the baseline model on the D_{mc} set and test them on the D split set ($D_{mc} \rightarrow D$). As shown in rows C1 and C2 of Table 2, compared to row A1, due to the new demonstration data being treated as interfering samples, the performance of the baseline method significantly declines (0.860 vs 0.821). In contrast, *RoboUniView* achieve significant improvements (0.954 vs 0.962 for task1, 0.461 vs 0.563 for task5) compared to row A2. This demonstrates that training across multiple datasets to enhance performance becomes possibility.

Joint Cross-task Learning for Cross-camera Parameters Generalization. The CALVIN [36] dataset includes 34 tasks. We segment the D split training set into two subsets based on task type: D_{train1} and D_{train2} , with each subset comprising 17 tasks. We change the camera parameters of D_{train2} , re-render the images based on demonstrations, and then merge them with D_{train1} to form the D_{jtmc} dataset. *RoboUniView* and the baseline models are trained on D_{jtmc} and test on all 34 tasks in the D split ($D_{jtmc} \rightarrow D$). As shown in rows D1 and D2 of Table 2, thanks to our strategy of decoupling visual feature extraction from action learning, our model significantly outperforms the baseline model (+0.012 vs -0.48). This demonstrates that our model can engage in joint cross-task learning across datasets with different camera parameters, leveraging the unified view representation.

4.4 Ablation Studies

Table 3: Ablation studies about UVFormer on the $D \rightarrow D$ dataset

UVFormer	Task Completed in a Sequence					Avg Len
	1	2	3	4	5	
U1 n/a (Baseline)	0.860	0.714	0.585	0.460	0.349	2.968
U2 Train (From Scratch)	0.893	0.763	0.613	0.491	0.408	3.168
U3 +Pre-train+Fine-tune	0.912	0.771	0.622	0.503	0.395	3.203
U4 +Pre-train+Fine-tune (Frozen)	0.954	0.827	0.685	0.564	0.461	3.491

UVFormer. UVFormer is the most critical component of our model, fundamentally determining the expression capability of the unified view representation. As shown in Table 3, we conduct thorough research: the first row U1 displays the baseline test results without UVFormer, the second row U2 shows the results after training our model directly on the $D \rightarrow D$ dataset; the third row U3 shows the results after pre-training UVFormer on the *Calvin_{rgb}* dataset followed by fine-tuning; the fourth row U4 shows the results when UVFormer is frozen during the fine-tuning process. Compared to the U1 baseline, the success rate of U2 increase from 0.860 to 0.893, demonstrating the importance of the UVFormer module and unified view representation. The success rates of U3 and U4 progressively increase to 0.954. These results indicate that the optimal performance of the model can be achieved by pre-training and freezing the UVFormer parameters during fine-tuning.

Table 4: Ablation studies on different resolutions of UniView Queries on the $D \rightarrow D$ dataset

Resolution(l, b, p)	Task Completed in a Sequence					Avg Len	Latency (ms)
	1	2	3	4	5		
(0.200, 0.200, 0.250)	0.865	0.710	0.560	0.412	0.314	2.861	98
(0.100, 0.100, 0.100)	0.902	0.761	0.614	0.481	0.381	3.139	101
(0.050, 0.050, 0.100)	0.893	0.763	0.613	0.491	0.408	3.168	105
(0.025, 0.025, 0.050)	0.906	0.760	0.615	0.491	0.412	3.184	205

Resolution of UniView Queries. We adjust the resolution of UniView Queries to explore its impact on model performance and speed. As shown in Table 4, with the resolution of UniView Queries increases, the performance of the model improves, but the latency of the model also increases. At resolutions below (0.050, 0.050, 0.100), the increase in resolution has minimal effect on latency. However, when the resolution increase to (0.025, 0.025, 0.050), the latency nearly doubles. To

balance the performance and speed of the model, we ultimately chose a resolution of (0.050, 0.050, 0.100). Casually speaking, the baseline latency is 91 milliseconds (ms).

5 Limitations and Future Work

Despite the introduction of the unified view representation, which enhances the robustness to camera parameters, this paper still faces some limitations. **Camera Calibration Dependency:** Our approach relies on precise camera calibration. This dependency means that any slight misalignment or calibration error could significantly affect the accuracy and reliability of the model’s output. Fortunately, camera calibration is a well-established and straightforward process, often involving the use of checkerboard or QR code patterns for calibration. **Simulation-Based Testing:** Due to the lack of real-robot data, this paper is not able to deploy on real-world robots, which is also the direction of our future work. It is promising to note that, with the exponential growth of robotic data, we are optimistic that future research will showcase *RoboUniView*’s effectiveness in real-world tasks.

6 Conclusion

This paper introduces *RoboUniView*, a novel visual-language model with a unified view representation for robotic manipulation, which proposes the pre-training method for this unified view representation. *RoboUniView* achieves state-of-the-art performance on benchmark datasets. Moreover, various experiments demonstrate our method’s significant generalization advantages with data from different camera parameters. These strengths clearly pave the way for our next objective: training a comprehensive embodied intelligence model on diverse robotic datasets to master all skills and deploy on various platforms.

References

- [1] Michael Ahn, Anthony Brohan, Noah Brown, Yevgen Chebotar, Omar Cortes, Byron David, Chelsea Finn, Chuyuan Fu, Keerthana Gopalakrishnan, Karol Hausman, et al. Do as i can, not as i say: Grounding language in robotic affordances. *arXiv preprint arXiv:2204.01691*, 2022.
- [2] Anas Awadalla, Irena Gao, Josh Gardner, Jack Hessel, Yusuf Hanafy, Wanrong Zhu, Kalyani Marathe, Yonatan Bitton, Samir Gadre, Shiori Sagawa, et al. Openflamingo: An open-source framework for training large autoregressive vision-language models. *arXiv preprint arXiv:2308.01390*, 2023.
- [3] Kevin Black, Mitsuhiko Nakamoto, Pranav Atreya, Homer Walke, Chelsea Finn, Aviral Kumar, and Sergey Levine. Zero-shot robotic manipulation with pretrained image-editing diffusion models. *arXiv preprint arXiv:2310.10639*, 2023.
- [4] Sid Black, Stella Biderman, Eric Hallahan, Quentin Anthony, Leo Gao, Laurence Golding, Horace He, Connor Leahy, Kyle McDonell, Jason Phang, et al. Gpt-neox-20b: An open-source autoregressive language model. *arXiv preprint arXiv:2204.06745*, 2022.
- [5] Anthony Brohan, Noah Brown, Justice Carbajal, Yevgen Chebotar, Xi Chen, Krzysztof Choromanski, Tianli Ding, Danny Driess, Avinava Dubey, Chelsea Finn, et al. Rt-2: Vision-language-action models transfer web knowledge to robotic control. *arXiv preprint arXiv:2307.15818*, 2023.
- [6] Anthony Brohan, Noah Brown, Justice Carbajal, Yevgen Chebotar, Joseph Dabis, Chelsea Finn, Keerthana Gopalakrishnan, Karol Hausman, Alex Herzog, Jasmine Hsu, et al. Rt-1: Robotics transformer for real-world control at scale. *arXiv preprint arXiv:2212.06817*, 2022.
- [7] Yigit Baran Can, Alexander Liniger, Danda Pani Paudel, and Luc Van Gool. Structured bird’s-eye-view traffic scene understanding from onboard images. In *Proceedings of the IEEE/CVF International Conference on Computer Vision*, pages 15661–15670, 2021.
- [8] Sudeep Dasari and Abhinav Gupta. Transformers for one-shot visual imitation. In *Conference on Robot Learning*, pages 2071–2084. PMLR, 2021.
- [9] Jia Deng, Wei Dong, Richard Socher, Li-Jia Li, Kai Li, and Li Fei-Fei. Imagenet: A large-scale hierarchical image database. In *2009 IEEE conference on computer vision and pattern recognition*, pages 248–255. Ieee, 2009.

- [10] Jacob Devlin, Ming-Wei Chang, Kenton Lee, and Kristina Toutanova. Bert: Pre-training of deep bidirectional transformers for language understanding. *arXiv preprint arXiv:1810.04805*, 2018.
- [11] Yiming Ding, Carlos Florensa, Pieter Abbeel, and Mariano Phielipp. Goal-conditioned imitation learning. *Advances in neural information processing systems*, 32, 2019.
- [12] Alexey Dosovitskiy, Lucas Beyer, Alexander Kolesnikov, Dirk Weissenborn, Xiaohua Zhai, Thomas Unterthiner, Mostafa Dehghani, Matthias Minderer, Georg Heigold, Sylvain Gelly, et al. An image is worth 16x16 words: Transformers for image recognition at scale. *arXiv preprint arXiv:2010.11929*, 2020.
- [13] Danny Driess, Fei Xia, Mehdi SM Sajjadi, Corey Lynch, Aakanksha Chowdhery, Brian Ichter, Ayzan Wahid, Jonathan Tompson, Quan Vuong, Tianhe Yu, et al. Palm-e: An embodied multimodal language model. *arXiv preprint arXiv:2303.03378*, 2023.
- [14] Chelsea Finn and Sergey Levine. Deep visual foresight for planning robot motion. In *2017 IEEE International Conference on Robotics and Automation (ICRA)*, pages 2786–2793. IEEE, 2017.
- [15] Ankit Goyal, Jie Xu, Yijie Guo, Valts Blukis, Yu-Wei Chao, and Dieter Fox. Rvt: Robotic view transformer for 3d object manipulation. In *Conference on Robot Learning*, pages 694–710. PMLR, 2023.
- [16] Xiuye Gu, Tsung-Yi Lin, Weicheng Kuo, and Yin Cui. Open-vocabulary object detection via vision and language knowledge distillation. *arXiv preprint arXiv:2104.13921*, 2021.
- [17] Abhinav Gupta, Adithyavairavan Murali, Dhiraj Prakashchand Gandhi, and Lerrel Pinto. Robot learning in homes: Improving generalization and reducing dataset bias. *Advances in neural information processing systems*, 31, 2018.
- [18] Sepp Hochreiter and Jürgen Schmidhuber. Long short-term memory. *Neural computation*, 9(8):1735–1780, 1997.
- [19] Yihan Hu, Jiazhi Yang, Li Chen, Keyu Li, Chonghao Sima, Xizhou Zhu, Siqi Chai, Senyao Du, Tianwei Lin, Wenhai Wang, et al. Planning-oriented autonomous driving. In *Proceedings of the IEEE/CVF Conference on Computer Vision and Pattern Recognition*, pages 17853–17862, 2023.
- [20] Wenlong Huang, Pieter Abbeel, Deepak Pathak, and Igor Mordatch. Language models as zero-shot planners: Extracting actionable knowledge for embodied agents. In *International Conference on Machine Learning*, pages 9118–9147. PMLR, 2022.
- [21] Eric Jang, Alex Irpan, Mohi Khansari, Daniel Kappler, Frederik Ebert, Corey Lynch, Sergey Levine, and Chelsea Finn. Bc-z: Zero-shot task generalization with robotic imitation learning. In *Conference on Robot Learning*, pages 991–1002. PMLR, 2022.
- [22] Bo Jiang, Shaoyu Chen, Qing Xu, Bencheng Liao, Jiajie Chen, Helong Zhou, Qian Zhang, Wenyu Liu, Chang Huang, and Xinggang Wang. Vad: Vectorized scene representation for efficient autonomous driving. In *Proceedings of the IEEE/CVF International Conference on Computer Vision*, pages 8340–8350, 2023.
- [23] Yunfan Jiang, Agrim Gupta, Zichen Zhang, Guanzhi Wang, Yongqiang Dou, Yanjun Chen, Li Fei-Fei, Anima Anandkumar, Yuke Zhu, and Linxi Fan. Vima: General robot manipulation with multimodal prompts. In *NeurIPS 2022 Foundation Models for Decision Making Workshop*, 2022.
- [24] Leslie Pack Kaelbling. The foundation of efficient robot learning. *Science*, 369(6506):915–916, 2020.
- [25] Siddharth Karamcheti, Suraj Nair, Annie S Chen, Thomas Kollar, Chelsea Finn, Dorsa Sadigh, and Percy Liang. Language-driven representation learning for robotics. *arXiv preprint arXiv:2302.12766*, 2023.
- [26] Tsung-Wei Ke, Nikolaos Gkanatsios, and Katerina Fragkiadaki. 3d diffuser actor: Policy diffusion with 3d scene representations. *arXiv preprint arXiv:2402.10885*, 2024.
- [27] Sergey Levine, Peter Pastor, Alex Krizhevsky, Julian Ibarz, and Deirdre Quillen. Learning hand-eye coordination for robotic grasping with deep learning and large-scale data collection. *The International journal of robotics research*, 37(4-5):421–436, 2018.

- [28] Xinghang Li, Minghuan Liu, Hanbo Zhang, Cunjun Yu, Jie Xu, Hongtao Wu, Chilam Cheang, Ya Jing, Weinan Zhang, Huaping Liu, et al. Vision-language foundation models as effective robot imitators. *arXiv preprint arXiv:2311.01378*, 2023.
- [29] Zhiqi Li, Wenhai Wang, Hongyang Li, Enze Xie, Chonghao Sima, Tong Lu, Yu Qiao, and Jifeng Dai. Bevformer: Learning bird’s-eye-view representation from multi-camera images via spatiotemporal transformers. In *European conference on computer vision*, pages 1–18. Springer, 2022.
- [30] Chuang Lin, Peize Sun, Yi Jiang, Ping Luo, Lizhen Qu, Gholamreza Haffari, Zehuan Yuan, and Jianfei Cai. Learning object-language alignments for open-vocabulary object detection. *arXiv preprint arXiv:2211.14843*, 2022.
- [31] Irena Linhartová, Ladislav Bumba, Jiří Mašín, Marek Basler, Radim Osíčka, Jana Kamanová, Kateřina Procházková, Irena Adkins, Jana Hejnová-Holubová, Lenka Sadílková, et al. Rtx proteins: a highly diverse family secreted by a common mechanism. *FEMS microbiology reviews*, 34(6):1076–1112, 2010.
- [32] Yingfei Liu, Tiancai Wang, Xiangyu Zhang, and Jian Sun. Petr: Position embedding transformation for multi-view 3d object detection. In *European Conference on Computer Vision*, pages 531–548. Springer, 2022.
- [33] Corey Lynch and Pierre Sermanet. Language conditioned imitation learning over unstructured data. *arXiv preprint arXiv:2005.07648*, 2020.
- [34] Jiageng Mao, Yuxi Qian, Hang Zhao, and Yue Wang. Gpt-driver: Learning to drive with gpt. *arXiv preprint arXiv:2310.01415*, 2023.
- [35] Oier Mees, Lukas Hermann, and Wolfram Burgard. What matters in language conditioned robotic imitation learning over unstructured data. *IEEE Robotics and Automation Letters*, 7(4):11205–11212, 2022.
- [36] Oier Mees, Lukas Hermann, Erick Rosete-Beas, and Wolfram Burgard. Calvin: A benchmark for language-conditioned policy learning for long-horizon robot manipulation tasks. *IEEE Robotics and Automation Letters*, 7(3):7327–7334, 2022.
- [37] Yao Mu, Qinglong Zhang, Mengkang Hu, Wenhai Wang, Mingyu Ding, Jun Jin, Bin Wang, Jifeng Dai, Yu Qiao, and Ping Luo. Embodiedgpt: Vision-language pre-training via embodied chain of thought. *Advances in Neural Information Processing Systems*, 36, 2024.
- [38] Suraj Nair, Eric Mitchell, Kevin Chen, Silvio Savarese, Chelsea Finn, et al. Learning language-conditioned robot behavior from offline data and crowd-sourced annotation. In *Conference on Robot Learning*, pages 1303–1315. PMLR, 2022.
- [39] Abhishek Padalkar, Acorn Pooley, Ajinkya Jain, Alex Bewley, Alex Herzog, Alex Irpan, Alexander Khazatsky, Anant Rai, Anikait Singh, Anthony Brohan, et al. Open x-embodiment: Robotic learning datasets and rt-x models. *arXiv preprint arXiv:2310.08864*, 2023.
- [40] Jonah Philion and Sanja Fidler. Lift, splat, shoot: Encoding images from arbitrary camera rigs by implicitly unprojecting to 3d. In *Computer Vision—ECCV 2020: 16th European Conference, Glasgow, UK, August 23–28, 2020, Proceedings, Part XIV 16*, pages 194–210. Springer, 2020.
- [41] Alec Radford, Jong Wook Kim, Chris Hallacy, Aditya Ramesh, Gabriel Goh, Sandhini Agarwal, Girish Sastry, Amanda Askell, Pamela Mishkin, Jack Clark, et al. Learning transferable visual models from natural language supervision. In *International conference on machine learning*, pages 8748–8763. PMLR, 2021.
- [42] Lennart Reiher, Bastian Lampe, and Lutz Eckstein. A sim2real deep learning approach for the transformation of images from multiple vehicle-mounted cameras to a semantically segmented image in bird’s eye view. In *2020 IEEE 23rd International Conference on Intelligent Transportation Systems (ITSC)*, pages 1–7. IEEE, 2020.
- [43] Tianhe Ren, Shilong Liu, Ailing Zeng, Jing Lin, Kunchang Li, He Cao, Jiayu Chen, Xinyu Huang, Yukang Chen, Feng Yan, et al. Grounded sam: Assembling open-world models for diverse visual tasks. *arXiv preprint arXiv:2401.14159*, 2024.
- [44] Ishika Singh, Valts Blukis, Arsalan Mousavian, Ankit Goyal, Danfei Xu, Jonathan Tremblay, Dieter Fox, Jesse Thomason, and Animesh Garg. Progprompt: Generating situated robot task plans using large language models. In *2023 IEEE International Conference on Robotics and Automation (ICRA)*, pages 11523–11530. IEEE, 2023.

- [45] Austin Stone, Ted Xiao, Yao Lu, Keerthana Gopalakrishnan, Kuang-Huei Lee, Quan Vuong, Paul Wohlhart, Sean Kirmani, Brianna Zitkovich, Fei Xia, et al. Open-world object manipulation using pre-trained vision-language models. *arXiv preprint arXiv:2303.00905*, 2023.
- [46] MN Team et al. Introducing mpt-7b: A new standard for open-source, commercially usable llms, 2023.
- [47] Hugo Touvron, Thibaut Lavril, Gautier Izacard, Xavier Martinet, Marie-Anne Lachaux, Timothée Lacroix, Baptiste Rozière, Naman Goyal, Eric Hambro, Faisal Azhar, et al. Llama: Open and efficient foundation language models. *arXiv preprint arXiv:2302.13971*, 2023.
- [48] Ashish Vaswani, Noam Shazeer, Niki Parmar, Jakob Uszkoreit, Llion Jones, Aidan N Gomez, Lukasz Kaiser, and Illia Polosukhin. Attention is all you need. *Advances in neural information processing systems*, 30, 2017.
- [49] Weiyao Wang, Yutian Lei, Gregory D Hage, and Liangjun Zhang. Vihe: Virtual in-hand eye transformer for 3d robotic manipulation. *arXiv preprint arXiv:2403.11461*, 2024.
- [50] Haoran Wei, Lingyu Kong, Jinyue Chen, Liang Zhao, Zheng Ge, Jinrong Yang, Jianjian Sun, Chunrui Han, and Xiangyu Zhang. Vary: Scaling up the vision vocabulary for large vision-language models. *arXiv preprint arXiv:2312.06109*, 2023.
- [51] Jimmy Wu, Rika Antonova, Adam Kan, Marion Lepert, Andy Zeng, Shuran Song, Jeannette Bohg, Szymon Rusinkiewicz, and Thomas Funkhouser. Tidybot: Personalized robot assistance with large language models. *Autonomous Robots*, 47(8):1087–1102, 2023.
- [52] Zhenhua Xu, Yujia Zhang, Enze Xie, Zhen Zhao, Yong Guo, Kenneth KY Wong, Zhenguo Li, and Hengshuang Zhao. Drivegpt4: Interpretable end-to-end autonomous driving via large language model. *arXiv preprint arXiv:2310.01412*, 2023.
- [53] Sarah Young, Dhiraj Gandhi, Shubham Tulsiani, Abhinav Gupta, Pieter Abbeel, and Lerrel Pinto. Visual imitation made easy. In *Conference on Robot Learning*, pages 1992–2005. PMLR, 2021.
- [54] Edwin Zhang, Yujie Lu, William Wang, and Amy Zhang. Language control diffusion: Efficiently scaling through space, time, and tasks. *arXiv preprint arXiv:2210.15629*, 2022.
- [55] Hongkuan Zhou, Zhenshan Bing, Xiangtong Yao, Xiaojie Su, Chenguang Yang, Kai Huang, and Alois Knoll. Language-conditioned imitation learning with base skill priors under unstructured data. *arXiv preprint arXiv:2305.19075*, 2023.
- [56] Wangchunshu Zhou, Yan Zeng, Shizhe Diao, and Xinsong Zhang. Vlua: A multi-task multi-dimension benchmark for evaluating vision-language pre-training. In *International Conference on Machine Learning*, pages 27395–27411. PMLR, 2022.
- [57] Xizhou Zhu, Weijie Su, Lewei Lu, Bin Li, Xiaogang Wang, and Jifeng Dai. Deformable detr: Deformable transformers for end-to-end object detection, 2021.